Journal of Power Sources 262 (2014) 414–420

Contents lists available at ScienceDirect

Journal of Power Sources

journal homepage: www.elsevier.com/locate/jpowsour

One-step synthesis of dopamine-derived micro/mesoporous nitrogen-doped carbon materials for highly efficient oxygen-reduction catalysts

Xuexia Liu [a,b], Hui Zhu [a], Xiurong Yang [a,*]

[a] State Key Laboratory of Electroanalytical Chemistry, Changchun Institute of Applied Chemistry, Chinese Academy of Sciences, Changchun, Jilin 130022, China
[b] University of the Chinese Academy of Sciences, Beijing 100039, China

HIGHLIGHTS

- Dopamine-derived micro/mesoporous nitrogen-doped carbon materials were synthesized.
- The carbon materials were fabricated by means of one step and green method.
- Showing excellent electrocatalytic activity for the oxygen reduction reaction.
- Showing superior stability to 20 wt% Pt/C catalyst.

ARTICLE INFO

Article history:
Received 13 December 2013
Received in revised form
3 April 2014
Accepted 4 April 2014
Available online 13 April 2014

Keywords:
Dopamine
Pyrolysis
Micro/mesoporous nitrogen-doped carbon
Oxygen reduction reaction

ABSTRACT

Micro/mesoporous nitrogen-doped carbon (*m*-NC) materials have been prepared by a simple one-step pyrolysis of dopamine in the presence of $FeCl_3$ at 350–750 °C. X-ray photoelectron spectroscopy (XPS) N 1s spectra indicate three types of C–N bonding patterns: graphitic N, pyrrolic N and pyridinic N. The electrocatalytic properties towards oxygen reduction reaction were investigated in alkaline media. Results indicated that the *m*-NC-600 with the highest content of pyridinic N and graphitic N showed improved electrocatalytic activity for the oxygen reduction reaction (ORR) in terms of onset potential, number of electron transferred and limiting current density. Moreover, the durability in alkaline media of the as-prepared *m*-NC-600 catalyst was found to be superior to the commercial Pt/C catalyst.

1. Introduction

Owing to the ever-increasing demands of fossil fuels, tremendous efforts have been focused on searching for sustainable and renewable sources of energy [1,2]. Fuel cells are considered to be a common type of energy conversion devices, developing for future energy applications. The proton-exchange membrane fuel cells (PEMFCs) are a promising candidate for applications in transportation vehicles, stationary grids and portable electronic devices among different types of fuel cells due to their own features, including modular and scalable properties, high efficient and lightweight [2,3]. Unfortunately, the oxygen reduction reaction (ORR) is one of the most crucial factors in determining the performance of PEMFCs [4–6]. Nowadays, sluggish kinetics of ORR at the cathode, the most technical bottleneck of fuel cells, hinders their widespread commercialization [7,8]. Platinum and its alloys have been regarded as the most effective cathode electrocatalysts for ORR [9]. Nevertheless, their high cost [10], limited supply [11] and weak durability [12] seriously hinder their large-scale applications. Thus, exploring of non-precious metals or even metal free catalysts is highly desirable.

Currently, several studies have demonstrated that heteroatom-doped carbon can effectively enhance ORR activity, such as nitrogen [13,14], boron [15], sulfur [16,17], phosphorous [18,19] and their mixtures [20,21]. Among them, the electron-enriched nitrogen-doped carbon materials can significantly enhance the number of active sites for improving ORR activity [22]. Up to now, many types of nitrogen-doped carbon materials including nitrogen-doped graphene [8,13,23], nitrogen-doped nanotubes [24,25] and nitrogen-doped carbon spheres [26,27] have been investigated as the ORR catalysts. Generally, nitrogen can be doped either directly during synthesis or by post-synthetic treatment [28]. However, post-doping approach often involves the preparation of carbon materials and then passing nitrogen-containing atmosphere at a

* Corresponding author. Tel.: +86 431 85262056; fax: +86 431 85689278.
E-mail address: xryang@ciac.ac.cn (X. Yang).

http://dx.doi.org/10.1016/j.jpowsour.2014.04.023
0378-7753/

high temperature, such as NH_3, N-ion plasma [29]. Moreover, this method requires multi-step process, high-cost hardware and obtained only surface functionalization [28,30,31]. Alternatively, in the *in situ* doping route, using various nitrogen-containing precursors yields the homogenous incorporation of nitrogen throughout the entire carbon materials [28]. For example, Antonietti's group has prepared high surface area porous carbons with ionic liquids (ILs) as precursors [32,33]. In addition, nitrogen-containing precursors also include low-vapor-pressure polymeric species (polypyrrole [28], polyacrylonitrile [34], polyaniline [35], etc.) [36]. Despite recent improvements, there still exist some problems in the preparation of carbon materials. Firstly, the pursuit of nontoxic carbon resources instead of poisonous compounds (ethylenediamine, pyridine, diaminopropane) is highly desirable, and this would be of great benefit both to humans and environment [14]. Secondly, the multiple steps in the preparation of polymers or ILs would complicate their manufacture and unavoidably hinder their large-scale applications [36]. Thus, it is challenging but highly desirable to explore a simple and green strategy to synthesize nitrogen-doped carbon materials with excellent ORR activity from low toxicity precursors.

With this point of view, we present a one-step method to prepare *m*-NC materials directly from the monomers of conducting polymers, using biomolecule dopamine as the carbon precursor. Compared with pyridine, dopamine is nontoxic, widespread and a sustainable resource. Very recently, carbon spheres have been prepared by polymerizing dopamine in solution, followed by carbonization [27]. However, this approach requires a multistep synthesis process. Herein, dopamine was mixed with $FeCl_3$ and then treated at different temperatures under argon atmosphere. After complete purifying, the obtained products were denoted by *m*-NC-*T* (where *T* is the temperature in degrees Celsius: 350, 400, 450, 500, 550, 600, 650 and 750 °C). The obtained products exhibited satisfactory electrocatalytic activity for the ORR. Moreover, the effect of different type nitrogen on the ORR was investigated based on XPS and ORR kinetic analysis. It was found that the *m*-NC-600 outperformed other *m*-NC-*T* catalysts in the ORR electrocatalytic activity.

2. Experimental

2.1. Reagents and apparatus

Dopamine was purchased from Sigma. Iron chloride anhydrous ($FeCl_3$) was obtained from Aladdin. Potassium hydroxide (KOH) and 36% HCl were brought from Beijing Chemical Reagent Company. All reagents were of analytical grade and used as received without further purification. Double-distilled (DI) water from a Millipore system (>18 MΩ cm) was employed throughout the experiment.

Transmission electron microscopy (TEM) was carried out with JEM-2000 FX operating at 200 kV accelerating voltage and scanning electron microscopy (SEM) images were taken using Philips XL 30 and a JEOL JSM-6700F microscope. X-ray photoelectron spectroscopy (XPS) measurements were performed on an ESCALAB MK II photoelectron spectrometer (VG Co., UK) with Al Kα X-ray radiation as the X-ray source for excitation. X-ray diffraction (XRD) analysis was carried out on a D/Max 2500V/PC X-ray diffractometer using Cu radiation. The surface area was calculated using the Brunauer–Emmett–Teller (BET) method based on adsorption data in the relative pressure (P/P_0) range of 0.06–0.14 and the total pore volume was determined from the amount of nitrogen adsorbed at a relative pressure (P/P_0) of 0.99. The pore size distribution (PSD) was determined *via* a nonlocal density functional theory (NL-DFT) method using nitrogen adsorption data.

2.2. Synthesis of m-NC-T materials

In an optimized synthesis, dopamine and $FeCl_3$ at a mass ratio of 1:5 were mixed and pressed together. Then, the mixture was heated in a tube furnace at different temperature (350–750 °C) for 6 h under argon flow. Subsequently, the resulting product, referred as *m*-NC-*T*, was washed with 2 M HCl and DI water to remove any metal residuals. For comparison, the carbon was also prepared by directly annealing dopamine at the temperature of 600 °C without $FeCl_3$ (denoted as dC-600).

2.3. Preparation of m-NC-T modified electrode and electrochemical measurements

Prior to use, the glassy carbon electrode (GCE, $\Phi = 5$ mm) was polished with 1.0 μm, 0.3 μm and 0.05 μm alumina/water slurry on a polishing cloth to a mirror-like finish, respectively, and rinsed thoroughly with ethanol solution and DI water in an ultrasonic bath. Then, the electrode was dried with blowing nitrogen gas. After that, a 15 μL aqueous dispersion of the *m*-NC-*T* (1.5 mg mL^{-1}) was dropped on a GCE and allowed to dry in air, and then 10 μL Nafion aqueous solution (0.05 wt%) was coated and air-dried. Linear sweep voltammetry (LSV) was performed using a computer-controlled 832 electrochemical analyzer (CH Instrument, Inc.) in a standard three-electrode system with 0.1 M KOH as electrolyte. The results of current–time chronoamperometric were obtained at +0.67 V *vs.* RHE in 0.1 M KOH solution with continuous oxygen bubbling at a rotation rate of 1600 rpm. N_2 or O_2 was used to purge the solution to achieve oxygen-free or oxygen-saturated electrolyte solution. Glassy carbon rotating disk electrode (RDE) was used as the working electrode. A Ag/AgCl (saturated potassium chloride) was used as the reference electrode and was calibrated with respect to a reversible hydrogen electrode (RHE) by adding 0.97 V (the potential of the Ag/AgCl reference measured against RHE). A platinum foil was used as the counter electrode. RDE experiments were carried out on an MSRX electrode rotator (Pine Instrument).

3. Results and discussion

3.1. Characterization of m-NC-T materials

The morphology of *m*-NC-600 was investigated by means of SEM. As shown in Fig. 1c and Fig. S1c, multilayer assemblies were discovered, which would provide a unique open-pore system and a short diffusion path for electrolyte ions [36,37]. The morphologies of other products obtained at 350, 550 and 750 °C were also characterized by SEM (Fig. S1a, b and d). No obvious changes were observed in morphology, and they all remained multilayer assembled structures. Fig. 1a and b depicted TEM images, it was to be noted that the *m*-NC-600 had the thin planar/lamellar structure. The microstructure of *m*-NC-600 was further characterized by high-resolution TEM (HRTEM) technique. As shown in Fig. S2, short and disordered graphite layer for the *m*-NC-600 could be observed. Both of these characterizations proved the successful synthesis of dopamine-derived carbon materials with the thin planar/lamellar morphology.

We conducted N_2 sorption isothermal analysis to investigate the porous properties (Fig. 1d). The typical nitrogen adsorption/desorption isotherms of *m*-NC-*T* materials belonged to the combined type I/IV isotherms according to the IUPAC classification. Besides, the H4-type hysteresis loop indicated the existence of micro/mesopores in the architectures. Fig. S3 displayed the pore size distributions of *m*-NC-*T* materials obtained using nonlocal density functional theory (NL-DFT) and the N_2 sorption data were

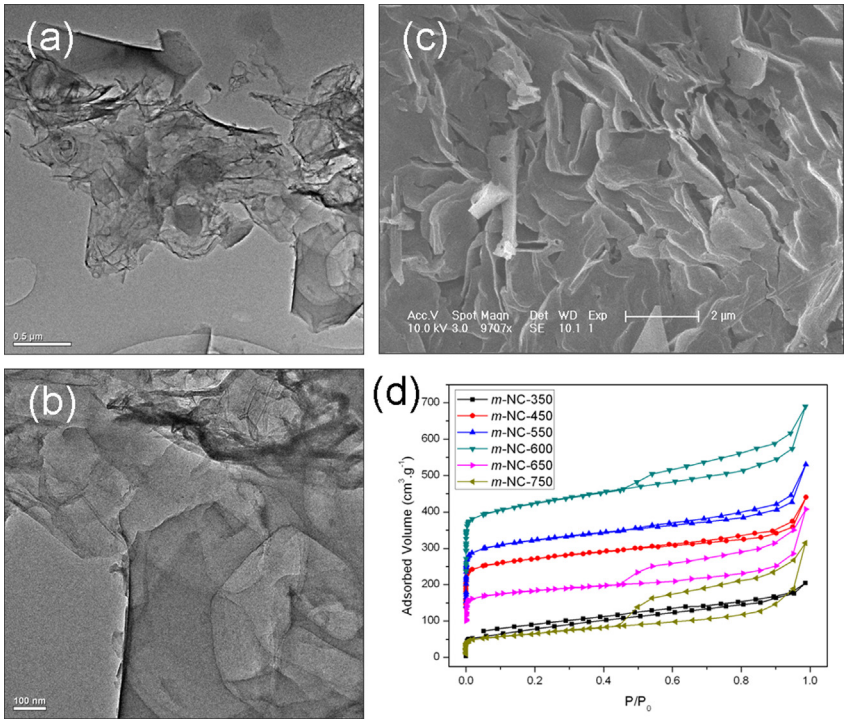

Fig. 1. (a and b) TEM and (c) SEM images of *m*-NC-600. (d) N_2 sorption isotherms of *m*-NC-*T* products.

summarized in Table 1. It was found that the specific surface area and total pore volume of *m*-NC-*T* materials were affected by the carbonization temperature. The *m*-NC-550 and *m*-NC-600 products exhibited larger specific surface area and total pore volume among the obtained products. Moreover, the surface area was also larger than many other reported nitrogen-doped carbon materials obtained from other precursors [14,36,38]. The aforementioned results demonstrated that the obtained carbon materials displayed excellent porous characteristics. In addition, the typical nitrogen adsorption/desorption isotherm of dC-600 was shown in Fig. S4. The specific surface area was lower than the detection limit of the instrument. The pore size distribution could not be determined *via* a nonlocal density functional theory method. We could conclude that $FeCl_3$ promoted the porosity of the products. Thus, it was reasonable to conclude that the micro/mesopores were generated on the layer architectures, which were expected to facilitate oxygen reduction reaction [39].

Fig. 2a showed the XRD patterns in the wide-angle region for the obtained products. A peak at about $2\theta = 26°$, could be assigned as the (002) diffraction peak of graphite. The broadening peak suggested a low graphitization degree, and thus the degree of graphitization became enhanced with the increase of the pyrolysis temperature. With ongoing graphitization, the (100) diffraction peak around 43.5° was appeared, informing a high degree of interlayer condensation, which induced a lower pore volume and surface area [40]. This result was coincident with the observation from BET. In addition, compared with dC-600, the *m*-NC-600 exhibited high degree of graphitization (Fig. 2a), indicating that $FeCl_3$ could promote the graphitization.

Table 1
Porous properties of *m*-NC-*T* products.

Sample name	S_{BET}[a] ($m^2\ g^{-1}$)	S_{mic}[b] ($m^2\ g^{-1}$)	S_{mes}[c] ($m^2\ g^{-1}$)	V_{pore}[d] ($cm^3\ g^{-1}$)
m-NC-350	285.1	34.29	250.81	0.3179
m-NC-450	718	520	198	0.559
m-NC-550	916.9	691	225.9	0.698
m-NC-600	855.7	530.3	325.4	0.747
m-NC-650	378.2	239	139.2	0.5077
m-NC-750	232.7	58.49	174.21	0.4885

[a] Specific surface area from multiple BET method.
[b] Micropore surface area from *t*-plot method.
[c] *t*-method external surface area ($S_{mes} = S_{BET} - S_{mic}$).
[d] Total pore volume at $P/P_0 = 0.99$.

To probe the chemical composition and the content of nitrogen in the *m*-NC-*T* materials, XPS analyses were performed. As expected, the wide scan spectra revealed the presence of C, N and O, without any other signals (Fig. 2b). The peak at 284 eV could be attributed to C 1s photoelectron excitation. The peak around 400 eV assigned to N 1s was observed, revealing the successful doping of nitrogen. As shown in Table S1, the content of carbon, oxygen and nitrogen elements changed following the variation of the reaction temperature. The obtained *m*-NC-*T* products exhibited higher oxygen content at low temperature because of the oxidative polymerization. The oxygen content was reduced gradually with the increase of the pyrolysis temperature, owing to the carbonization. Thus, $FeCl_3$ could oxidize the polymerization at the initial stage and then catalyze the graphitization at high temperature [36]. It was worthwhile to note that the overall nitrogen content in the *m*-NC-*T* materials also depended on the reaction temperature. For example, the nitrogen content for *m*-NC-550 was 3.42 at.%, while it reduced to 0.97 at.% for *m*-NC-650. The high-resolution N 1s XPS spectra were given in Fig. 3 and the types of nitrogen species were identified by the curve-fitting method with XPS peak-fit software. The spectra of N 1s peak could be deconvoluted into three types: 398.5, 400.1 and 401.2 eV, corresponding to the pyridinic N, pyrrolic N and graphitic N, respectively [8,41,42]. When the reaction temperature reached 650 °C, the spectra of N 1s peak could not be fitted into three peaks due to the low content of nitrogen. Table 2 showed the quantitative analysis results of pyridinic N, pyrrolic N and graphitic N in *m*-NC-450, *m*-NC-550, *m*-NC-600 and *m*-NC-650. The difference in the amount of N-bonding species was attributed to the

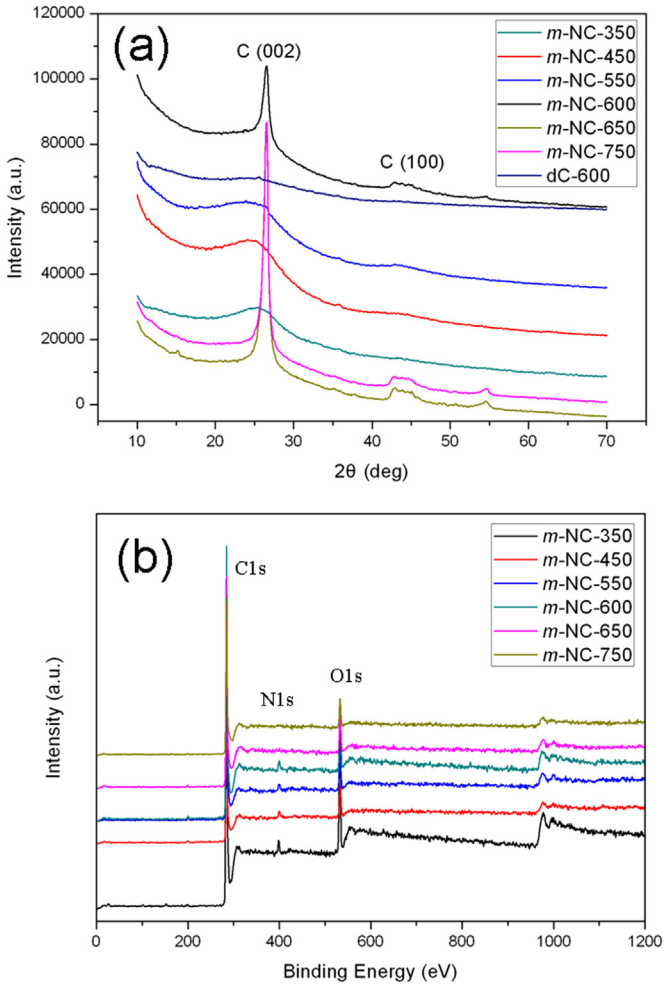

Fig. 2. (a) XRD results and (b) XPS spectra of as-prepared *m*-NC-*T* products.

different pyrolysis temperatures. Therefore, we have successfully synthesized the *m*-NC-600 product with high proportion of pyridinic N and graphitic N, which could improve electrocatalytic activity for ORR, because these two types of nitrogen-doped carbon species played an important role as active sites for ORR [43–45].

3.2. Electrocatalytic activity of m-NC-T materials towards ORR in alkaline medium

To evaluate the different electrocatalytic performance of our products towards ORR, linear sweep voltammograms (LSVs) were carried out with a three-electrode system in O_2-saturated 0.1 M KOH solution at a scan rate of 10 mV s^{-1} between −0.03 and +1.17 V *vs.* RHE. For comparison, the LSVs of different catalysts with a rotation rate of 1600 rpm were shown in Fig. 4b. In terms of limiting current densities, the value of *m*-NC-600 was higher than other products, but still lower than that of 20 wt% Pt/C. Additionally, the onset potential for 20 wt% Pt/C was around +1.01 V *vs.* RHE, whereas the corresponding onset potential of the *m*-NC-600 was shifted negatively to about +0.92 V *vs.* RHE, but more positive than that of the *m*-NC-*T* materials obtained at other temperatures and dC-600. On the basis of onset potential, the positive shift informed that the *m*-NC-600 had a lower ORR over-potential, thereby enhancing electrocatalytic activity [46]. Remarkably, the *m*-NC-600 exhibited the most positive half-wave potential (i.e. the potential at which the current is half of the limiting current) among the products, which was a 68 mV negative shift compared with 20 wt% Pt/C, further confirming that the *m*-NC-600 had excellent electrocatalytic activity for ORR in comparation with other *m*-NC-*T* materials and may have more active sites towards ORR [47]. Furthermore, in terms of the onset potential, number of electron transferred (Fig. 4d) and current density for ORR, the obtained *m*-NC-600 product exhibited superior electrocatalytic activity compared with other carbon materials obtained using nitrogen-containing aromatic polymers and organics (polyaniline [38,48], 1,3-diaminopropane and 1,4-diaminobutane [49], iron 1,10-phenanthroline [50], pyridine [51]) as the precursors. For example, the onset potential and number of electron transferred for polyaniline were +0.82 V *vs.* RHE and 2.5, which were both lower than that of the obtained *m*-NC-600 product. Moreover, the *m*-NC-600 displayed kinetic-limiting current density of 10.54 mA cm^{-2} at the potential of +0.57 V *vs.* RHE (Fig. 4d), significant superior to 1.02 mA cm^{-2} (−0.2 V *vs.* Ag/AgCl), 0.65 mA cm^{-2} (−0.2 V *vs.* Ag/AgCl) and 4.97 mA cm^{-2} (−0.35 V *vs.* Ag/AgCl) determined for 1,3-diaminopropane, 1,4-diaminobutane and pyridine, respectively. Thus, we have developed a simple one-step and green method to synthesis the *m*-NC-600 product with excellent electrocatalytic activity for ORR.

Obviously, the ORR activity was dependent on the pyrolysis temperature and the optimum temperature appeared to be 600 °C. The higher electrocatalytic performance of the *m*-NC-600 compared with other *m*-NC-*T* materials for ORR could be attributed to the different degree of graphitization and the different content of nitrogen, especially the proportion of pyridinic N and graphitic N in the obtained products, which played a key role for the enhanced electrocatalytic activity [14,26,43–45]. As depicted in Table S1 and Table 2, the higher nitrogen, pyridinic N and graphitic N content in the *m*-NC-600 were evidenced, which were in consistent with its higher electrocatalytic activity. It has been reported that the introduced N could also effectively enhance the ORR electrocatalytic activity of carbon [8,52,53]. In detail, pyridinic N with strong electron-accepting ability could create positive charge on the adjacent carbon atoms and the relatively electronegative graphitic N could also reduce the electron density on the adjacent C nuclei, which not only facilitated O_2 adsorption, but also helped attracting electrons from the anode, thus improving the ORR activity [14,52,54,55]. Therefore, combined with the high surface area and micro/mesoporous properties, such a doping nature could improve the electrocatalytic activity of the *m*-NC-600 for ORR.

LSVs recorded on different rotation rate were shown in Fig. 4a and Fig. S5. The limiting current densities significantly increased with rotation rates from 225 to 2500 rpm due to high rotation rates leading to a faster oxygen flux to electrode surface and consequently larger currents [56,57]. For further insights into ORR mechanism on different electrode, the kinetic parameters can be analyzed on the basis of the Koutecky–Levich (K–L) equations [58]:

$$1/j = 1/j_l + 1/j_k = 1/\left(B\omega^{1/2}\right) + 1/j_k \quad (1)$$

$$B = 0.62nFC_0(D_0)^{2/3}\nu^{-1/6} \quad (2)$$

$$j_k = nFkC_0 \quad (3)$$

where j, j_k, j_l represent the measured, kinetic and diffusion-limiting current densities, respectively. ω is the angular velocity of the disk ($\omega = 2\pi N$, N is the linear rotation rate), n is the overall number of electron transferred during the oxygen reduction reaction. F is the Faraday constant ($F = 96\,485$ C mol^{-1}), C_0 is the bulk concentration of O_2 ($C_0 = 1.2 \times 10^{-3}$ mol L^{-1}), D_0 is the diffusion coefficient of O_2 in the KOH electrolyte ($D_0 = 1.9 \times 10^{-5}$ cm^2 s^{-1}), ν is the kinematic

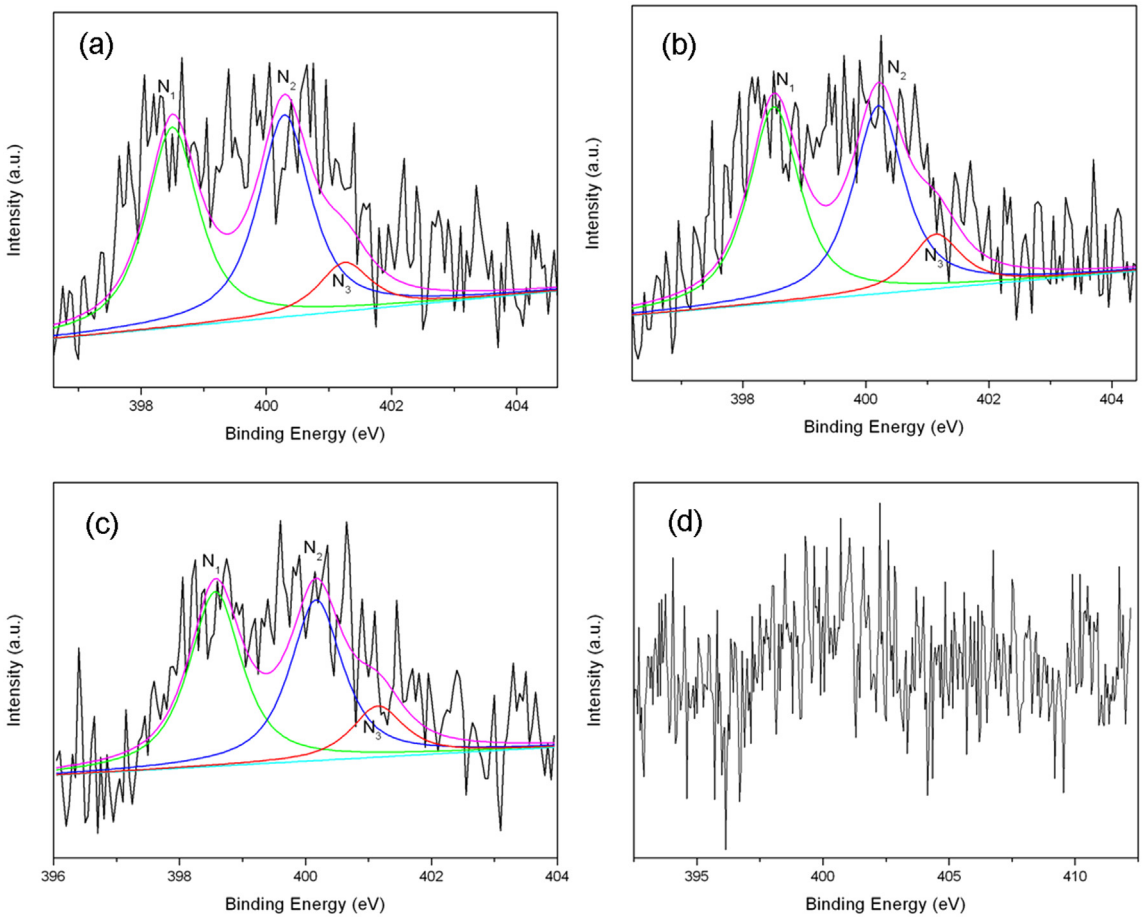

Fig. 3. N 1s XPS spectra of (a) *m*-NC-450, (b) *m*-NC-550, (c) *m*-NC-600 and (d) *m*-NC-650 (pyridinic (N1), pyrrolic (N2) and graphitic type nitrogen (N3)).

viscosity of the electrolyte ($\nu = 0.01$ cm^2 s^{-1} in 0.1 M KOH), and k is the electron-transfer rate constant. Fig. 4c and Fig. S6 depict the K–L curves for all *m*-NC-*T* catalysts. All plots give good linearity and parallelism, informing the consistent electron-transfer at different potentials and the first-order reaction kinetics for ORR with respect to the concentration of dissolved O_2 [29,57,59]. The value of n for the *m*-NC-600 is around four in the full potential range, implying that four-electron reduction of O_2 at lower over-potential is achieved [60].

The reduction of O_2 in alkaline solutions proceeded *via* either a direct four-electron pathway [61]

$$O_2 + 2H_2O + 4e^- \rightarrow 4OH^- \quad (4)$$

or a two-electron pathway

$$O_2 + 2H_2O + 2e^- \rightarrow HO_2^- + OH^- \quad (5)$$

Table 2
The relative atomic ratios of three nitrogen species (N1, N2 and N3).[a]

Sample name	N1 content (atomic%)	N2 content (atomic%)	N3 content (atomic%)	N content (atomic%)
m-NC-450	1.07	1.1	0.26	2.43
m-NC-550	1.53	1.47	0.42	3.42
m-NC-600	1.56	1.44	0.47	3.47
m-NC-650	–	–	–	0.97

[a] Hydrogen is not taken into account for the calculation.

According to Equations (1) and (2), the number of electron transferred (n) and kinetic-limiting current densities (j_k) at different potentials can be obtained from the slop and the intercept of the K–L plots. As shown in Fig. 4d, the n values for ORR were calculated to be 2.05, 1.21, 3.13, 3.3, 3.35, 3.61, 2.25, 1.89, 2.23 for *m*-NC-350, *m*-NC-400, *m*-NC-450, *m*-NC-500, *m*-NC-550, *m*-NC-600, *m*-NC-650, *m*-NC-700, and *m*-NC-750 at the potential of +0.57 V *vs.* RHE, respectively. In addition, compared with other *m*-NC-*T* catalysts, the *m*-NC-600 exhibited highest kinetic-limiting current density of 10.54 mA cm^{-2}. The near four-electron transfer pathway and high kinetic-limiting current density further confirmed the excellent ORR electrocatalytic activity of the *m*-NC-600 material in alkaline media. Our experimental results approved that the higher nitrogen, pyridinic N and graphitic N content, high BET surface area and micro/mesoporous properties could result in improving electrocatalytic activity for ORR.

Furthermore, the durabilities of the *m*-NC-600 and 20 wt% Pt/C catalysts toward ORR were evaluated by current–time (j–t) chronoamperometry at a constant potential of +0.67 V *vs.* RHE for 20 000 s in an O_2-saturated 0.1 M KOH solution. This result was shown in Fig. 5. The chronoamperometric response for the *m*-NC-600 exhibited much slower attenuation than that of 20 wt% Pt/C catalyst, and a high relative current 86% for the *m*-NC-600 was still persisted after reaction for 20 000 s. In contrast, only about 75% of the initial current density was maintained for 20 wt% Pt/C catalyst. The result confirmed that, beyond the excellent electrocatalytic activity, the *m*-NC-600 material exhibited a much better stability than commercial 20 wt% Pt/C catalyst in alkaline solution, which

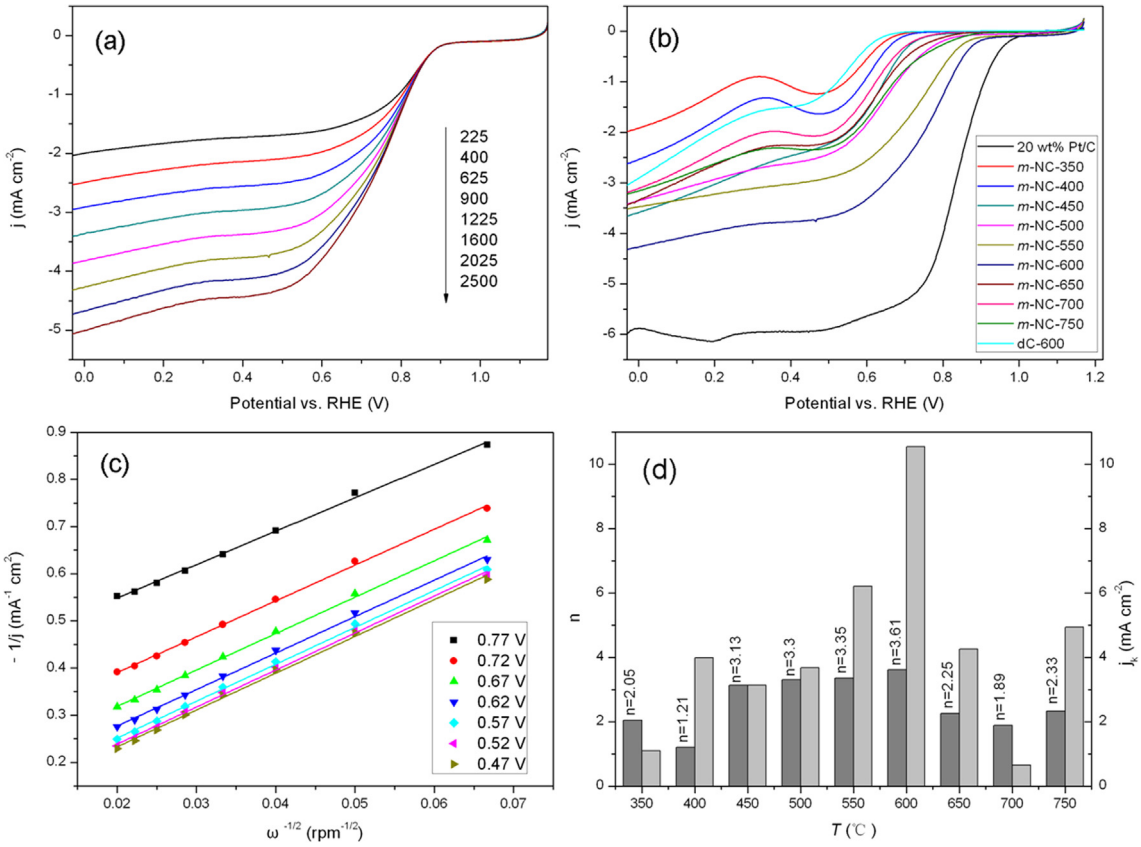

Fig. 4. (a) LSVs of *m*-NC-600/GCE in O_2-saturated 0.1 M KOH solution with various rotation rates at a scan rate of 10 mV s^{-1}. (b) Comparative LSVs at 1600 rpm for *m*-NC-*T* products, dC-600 and 20 wt% Pt/C. (c) Koutecky–Levich plots of *m*-NC-600/GCE derived from LSVs in (a) at different electrode potentials. (d) Comparison of electron transfer numbers (*n*) for as-prepared *m*-NC-*T* products with electrochemical activity given as the kinetic-limiting current densities (j_k) at +0.57 V *vs.* RHE.

made it a very promising cathode catalyst for the development of alkaline fuel cells [22].

4. Conclusions

In summary, we have developed an integrated one-step and green approach for fabricating micro/mesoporous nitrogen-doped carbon materials. In this method, dopamine was used as the carbon precursor owing to its biocompatibility. Throughout the synthesis process, $FeCl_3$ played important roles, including oxidizing the polymerization of the monomers and promoting the graphitization and porosity. Due to the high degree of graphitization and the high proportion of pyridinic N and graphitic N, the obtained *m*-NC-600 product exhibited excellent electrocatalytic activity for ORR in alkaline solution. Apart from these properties, the high surface area of the *m*-NC-600 product resulting from the micro/mesoporous structure also made a contribution to the high electrocatalytic activity for ORR. For the details, the good electrocatalytic activity of the *m*-NC-600 was confirmed by a more positive onset potential of +0.92 V *vs.* RHE, near four-electron reduction of O_2 at lower over-potential and highest kinetic-limiting current density of 10.54 mA cm^{-2} at +0.57 V *vs.* RHE. In addition, compared with the commercial 20 wt% Pt/C catalyst, the *m*-NC-600 product showed superior stability, which was favored for fuel cell applications.

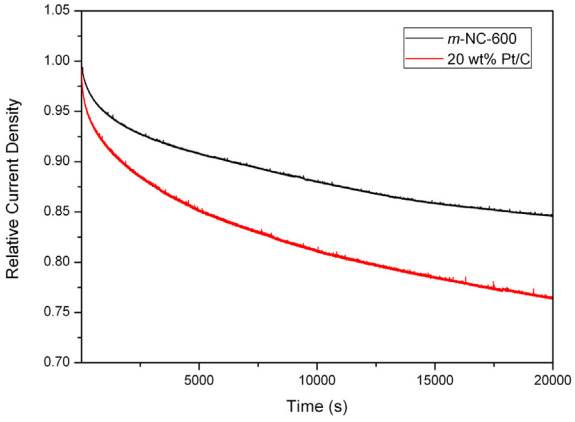

Fig. 5. Chronoamperometric responses of *m*-NC-600 and 20 wt% Pt/C catalysts modified GCE, at +0.67 V *vs.* RHE in an O_2-saturated 0.1 M KOH solution at a rotation rate of 1600 rpm, which are normalized to the initial current responses.

Acknowledgments

This work was supported by the National Natural Science Foundation of China (No. 21175124 and No. 51202240) and the National Key Basic Research Development Project of China (No. 2010CB933602).

Appendix A. Supplementary data

Supplementary data related to this article can be found at http://dx.doi.org/10.1016/j.jpowsour.2014.04.023.

References

[1] S.J. Guo, S. Zhang, S.H. Sun, Angew. Chem. Int. Ed. 52 (2013) 8526–8544.
[2] R. Borup, J. Meyer, B. Pivovar, Y.S. Kim, R. Mukundan, N. Garland, D. Myers, M. Wilson, F. Garzon, D. Wood, P. Zelenary, K. More, K. Stroh, T. Zawodzinski, J.E. Macgrath, M. Inaba, K. Miyatake, M. Hori, K. Ota, Z. Ogumi, S. Miyata, A. Nishikata, Z. Siroma, Y. Uchimoto, K. Yasuda, K. Kimijima, N. Iwashita, Chem. Rev. 107 (2007) 3904–3951.
[3] H.J. Tang, H.J. Yin, J.Y. Wang, N.L. Yang, D. Wan, Z.Y. Tang, Angew. Chem. Int. Ed. 52 (2013) 5585–5589.
[4] S. Chen, J.Y. Bi, Y. Zhao, L.J. Yang, C. Zhang, Y.W. Ma, Q. Wu, X.Z. Wang, Z. Hu, Adv. Mater. 24 (2012) 5593–5597.
[5] B.C.H. Steele, A. Heinzel, Nature 414 (2001) 345–352.
[6] W. Xiong, F. Du, Y. Liu, A. Perez Jr., M. Supp, T.S. Ramakrishnan, L.M. Dai, L. Jiang, J. Am. Chem. Soc. 132 (2010) 15839–15841.
[7] R.M. Darling, J.P. Meyers, J. Electrochem. Soc. 150 (2003) A1523–A1527.
[8] D.S. Geng, Y. Chen, Y.G. Chen, Y.L. Li, R.Y. Li, X.L. Sun, S.Y. Ye, S. Knights, Energy Environ. Sci. 4 (2011) 760–764.
[9] B.Z. Fang, N.K. Chaudhari, M.S. Kim, J.H. Kim, J.S. Yu, J. Am. Chem. Soc. 131 (2009) 15330–15338.
[10] C. Xiong, Z.D. Wei, B.S. Hu, S.G. Chen, L. Li, L. Guo, W. Ding, X. Liu, W.J. Ji, X.P. Wang, J. Power Sources 215 (2012) 216–220.
[11] W. Chen, S.W. Chen, Angew. Chem. Int. Ed. 121 (2009) 4450–4453.
[12] Y.Y. Shao, J. Liu, Y. Wang, Y.H. Lin, J. Mater. Chem. 19 (2009) 46–59.
[13] Z.H. Sheng, L. Shao, J.J. Chen, W.J. Bao, F.B. Wang, X.H. Xia, ACS Nano 5 (2011) 7752–7777.
[14] H. Wang, X.J. Bo, C. Luhana, L.P. Guo, Electrochem. Commun. 21 (2012) 5–8.
[15] L.J. Yang, S.J. Jiang, Y. Zhao, L. Zhu, S. Chen, X.Z. Wang, Q. Wu, J. Ma, Y.W. Ma, Z. Hu, Angew. Chem. Int. Ed. 50 (2011) 7132–7135.
[16] S. Inamdar, H.S. Choi, P. Wang, M.Y. Song, J.S. Yu, Electrochem. Commun. 30 (2013) 9–12.
[17] Z. Yang, Z. Yao, G.F. Li, G.Y. Fang, H.G. Nie, Z. Liu, X.M. Zhou, X.A. Chen, S.M. Huang, ACS Nano 6 (2012) 205–211.
[18] D.S. Yang, D. Bhattacharjya, S. Inamdar, J. Park, J.S. Yu, J. Am. Chem. Soc. 134 (2012) 16127–16130.
[19] Y. Kim, Y. Park, A. Choi, N.S. Choi, J. Kim, J. Lee, J.H. Ryu, S.M. Oh, K.T. Lee, Adv. Mater. 25 (2013) 3045–3049.
[20] C.H. Choi, S.H. Park, S.I. Woo, ACS Nano 6 (2012) 7084–7091.
[21] Y. Zhao, L.J. Yang, S. Chen, X.Z. Wang, Y.W. Ma, Q. Wu, Y.F. Jiang, W.J. Qian, Z. Hu, J. Am. Chem. Soc. 135 (2013) 1201–1204.
[22] Y.M. Tan, C.F. Xu, G.X. Chen, X.L. Fang, N.F. Zheng, Q.J. Xie, Adv. Funct. Mater. 22 (2012) 4584–4591.
[23] B. Zheng, J. Wang, F.B. Wang, X.H. Xia, Electrochem. Commun. 28 (2013) 24–26.
[24] Z.Y. Mo, S.J. Liao, Y.Y. Zheng, Z.Y. Fu, Carbon 50 (2012) 2620–2627.
[25] Z. Chen, D. Higgins, Z.W. Chen, Carbon 48 (2010) 3057–3065.
[26] Y. Li, T.T. Li, M. Yao, S.Q. Liu, J. Mater. Chem. 22 (2012) 10911–10917.
[27] K.L. Ai, Y.L. Liu, C.P. Ruan, L.H. Lu, G.Q. Lu, Adv. Mater. 25 (2013) 998–1003.
[28] M. Sevilla, L.H. Yu, T.P. Fellinger, A.B. Fuertes, M.M. Titirici, RSC Adv. 3 (2013) 9904–9910.
[29] S. Shanmugam, T. Osaka, Chem. Commun. 47 (2011) 4463–4465.
[30] M.M. Titirici, A. Thomas, M. Antonietti, J. Mater. Chem. 17 (2007) 3412–3418.
[31] L.Q. Jiang, L. Gao, Carbon 41 (2003) 2923–2929.
[32] J.P. Paraknowitsch, J. Zhang, D.S. Su, A. Thomas, M. Antonietti, Adv. Mater. 22 (2010) 87–92.
[33] T.P. Fellinger, F. Hasché, P. Strasser, M. Antonietti, J. Am. Chem. Soc. 134 (2012) 4072–4075.
[34] A.H. Lu, A. Kiefer, W. Schmidt, F. Schüth, Chem. Mater. 16 (2004) 100–103.
[35] C. Jeyabharathi, P. Venkateshkumar, M.S. Rao, J. Mathiyarasu, K.L.N. Phani, Electrochim. Acta 74 (2012) 171–175.
[36] H. Zhu, X.L. Wang, X.X. Liu, X.R. Yang, Adv. Mater. 24 (2012) 6524–6529.
[37] F. Beguin, E. Frackowiak, Carbons for Electrochemical Energy Storage and Conversion Systems, Taylor and Francis, Boca Raton, FL, 2010.
[38] N. Gavrilov, I.A. Pašti, M. Mitrić, J. Travas-Sejdić, G. Ćirić-Marjanović, S.V. Mentus, J. Power Sources 220 (2012) 306–316.
[39] J. Liang, Y. Jiao, M. Jaroniec, S.Z. Qiao, Angew. Chem. Int. Ed. 51 (2012) 11496–11500.
[40] J.S. Lee, X.Q. Wang, H.M. Luo, S. Deng, Adv. Mater. 22 (2010) 1004–1007.
[41] J.J. Wu, D. Zhang, Y. Wang, B.R. Hou, J. Power Sources 227 (2013) 185–190.
[42] L.Y. Feng, Y.G. Chen, L. Chen, ACS Nano 5 (2011) 9611–9618.
[43] J. Yin, Y.J. Qiu, J. Yu, J. Electrochem. Soc. 702 (2013) 56–59.
[44] P.H. Matter, U.S. Ozkan, Catal. Lett. 109 (2006) 115–123.
[45] G. Liu, X.G. Li, P. Ganesan, B.N. Popov, Appl. Catal. B – Environ. 93 (2009) 156–165.
[46] S. Yasuda, L. Yu, J. Kim, K. Murakoshi, Chem. Commun. 49 (2013) 9627–9629.
[47] X.M. Zhai, W. Yang, M.Y. Li, G.Q. Lv, J.P. Liu, X.L. Zhang, Carbon 65 (2013) 277–286.
[48] A. Janošević, I. Pašti, N. Gavrilov, S. Mentus, G. Ćirić-Marjanović, J. Krstić, J. Stejskal, Synth. Met. 161 (2011) 2179–2184.
[49] D. Higgins, Z. Chen, Z.W. Chen, Electrochim. Acta 56 (2011) 1570–1575.
[50] T. Onodera, T. Mizukami, S. Suzuki, J. Kawaji, K. Yamaga, T. Yamamoto, Catal. Commun. 43 (2014) 66–71.
[51] Z. Chen, D. Higgins, Z.W. Chen, Electrochim. Acta 55 (2010) 4799–4804.
[52] L.F. Lai, J.R. Potts, D. Zhan, L. Wang, C.K. Poh, C.H. Tang, H. Gong, Z.X. Shen, J.Y. Lin, R.S. Ruoff, Energy Environ. Sci. 5 (2012) 7936–7942.
[53] L.T. Qu, Y. Liu, J.B. Baek, L.M. Dai, ACS Nano 4 (2010) 1321–1326.
[54] D.S. Yu, Q. Zhang, L.M. Dai, J. Am. Chem. Soc. 132 (2010) 15127–15129.
[55] S. Kundu, T.C. Nagaiah, W. Xia, Y.M. Wang, S.V. Dommele, J.H. Bitter, M. Santa, G. Grundmeier, M. Bron, W. Schuhmann, M. Muhler, J. Phys. Chem. C. 113 (2009) 14302–14310.
[56] F.Y. Cheng, Y. Su, J. Liang, Z.L. Tao, J. Chen, Chem. Mater. 22 (2010) 898–905.
[57] H.B. Li, W.J. Kang, L. Wang, Q.L. Yue, S.L. Xu, H.L. Wang, J.F. Liu, Carbon 54 (2013) 249–257.
[58] M. Jahan, Q.L. Bao, K.P. Loh, J. Am. Chem. Soc. 134 (2012) 6707–6713.
[59] N.R. Elezović, B.M. Babić, L. Gajić-Krstajić, V. Radmilović, N.V. Krstajić, L.J. Vračar, J. Power Sources 195 (2010) 3961–3968.
[60] J.J. Wu, D. Zhang, Y. Wang, Y. Wan, Electrochim. Acta 75 (2012) 305–310.
[61] Z.W. Xu, H.J. Li, M.S. Fu, H.J. Luo, H.H. Sun, L.J. Zhang, K.Z. Li, B.Q. Wei, J.H. Lu, X.N. Zhao, J. Mater. Chem. 22 (2012) 18230–18236.